Eurasian Chemico-Technological Journal 20 (2018) 283-291

https://doi.org/10.18321/ectj761

Control of Ni/$Ce_{1-x}M_xO_y$ Catalyst Properties Via the Selection of Dopant M = Gd, La, Mg. Part 1. Physicochemical Characteristics

M.A. Kerzhentsev[1], E.V. Matus[1,2]*, I.Z. Ismagilov[1], O.B. Sukhova[1], P. Bharali[3], Z.R. Ismagilov[1,4]

[1]Boreskov Institute of Catalysis SB RAS, pr. Ak. Lavrentieva 5, 630090 Novosibirsk, Russia
[2]Novosibirsk State Technical University, pr. K. Marksa 20, 630073 Novosibirsk, Russia
[3]Tezpur University, Napaam, Tezpur - 784 028 Assam, India
[4]Institute of Coal Chemistry and Material Science FRC CCC SB RAS, pr. Sovetskiy 18, 650000 Kemerovo, Russia

Article info

Received:
15 March 2018

Received in revised form:
5 May 2018

Accepted:
23 July 2018

Keywords:
ceria
dopant
metal-support interaction
Ni catalyst
reforming

Abstract

To develop effective reforming catalyst a series of Ni catalysts (Ni content 2–15 wt.%) supported on ceria-based oxides $Ce_{1-x}M_xO_y$ were synthesized by incipient wetness impregnation. To regulate dispersion and reducibility of the active component, the variation of chemical composition of support was performed. The prepared samples of supports and catalysts were characterized by X-ray spectral fluorescence analysis, N_2 adsorption/desorption, X-ray diffraction, transmission electron microscopy, and thermal analysis. It was found that the support composition specified the forms of stabilization (NiO or Ni-M-O oxides, M = La, Mg) and capability to reduction of Ni-component through the realization of a different extent of interaction between Ni-containing species and support. The increase of M content in $Ce_xM_{1-x}O_y$ support induces the decrease of $Ce_xM_{1-x}O_y$ crystallite size, improvement of Ni active component dispersion and the increase of hard-to-reduce portion of nickel cations due to the growth in the degree of nickel-$Ce_xM_{1-x}O_y$ interaction. The identified variation of the textural, structural and redox characteristics of the Ni/$Ce_xM_{1-x}O_y$ catalysts should influence their performance in the catalytic process.

1. Introduction

Nickel-containing catalysts are effective catalytic systems for the conversion of hydrocarbons and oxygenates to hydrogen-containing gas [1–12]. Significant advantages of nickel catalysts include their high activity and their relatively low cost. However, under the conditions of the catalytic process, the sintering and oxidation of the phase of the active component as well as the formation of carbon deposits are possible [10, 13–15]. This leads to a gradual deactivation of the catalysts and determines their main disadvantages. Achieving improvement in the process parameters is possible by optimizing the dispersion and capability to reduction of the active component through varying the support composition [10, 14, 16], method and conditions of synthesis [15, 17, 18], type and content of the promoter [13, 19]; that is, by controlling the functional properties of the catalyst through directed regulation of its physicochemical characteristics.

The type and characteristics of supports can affect the structural and electronic properties of supported Ni species as well as take part in the transformation of reagents and intermediates. It was established [20] that MgO, ZnO, La_2O_3 and CeO_2 oxides with basic characteristics provide the long-term stability of Ni catalysts through the promotion of oxygenate dehydrogenation but inhibition of its dehydration. Lanthanum oxycarbonate formation from La_2O_3 support or high amount of mobile lattice oxygen in CeO_2 support are responsible for the removal of carbon deposits during fuel conversion over Ni-based catalysts [21]. $Ce_{1-x}M_xO_y$ solid solutions (M = Zr, La) are also widely used as supports for reforming catalyst due to their redox properties, high oxygen capacity and mobility, as well as the implementation of strong interaction between supported metal and carrier [6, 22–24]. The own

*Corresponding author. E-mail: matus@catalysis.ru

catalytic ability of CeO_2–based supports and mode of their interaction with the active component are affected by dopant type [6, 25, 26]. In particular, the presence of the dopant cations (Gd, La, Eu) in the CeO_2 lattice increases the concentration of structural oxygen vacancies and the reducibility of the redox pair Ce^{4+}/Ce^{3+}, which leads to higher catalytic activity in the CO oxidation reaction than that of undoped CeO_2 [25]. At the introduction of 12 mol.% La_2O_3 in the support composition of Co/Ce-La-O catalysts, the formation of the $Ce(La)O_x$ solid solution is observed that promotes the dispersion of metallic cobalt, decreases the coke deposits and increases the selectivity to H_2 in steam reforming of ethanol [27]. Rh-catalyst supported on the Ce-La solid solution with the molar ratio La/Ce+La = 0.3 has the highest reducibility that is proposed to correspond to the most abundant active sites for ethanol conversion [28]. So the development of appropriate support for reforming catalysts is an urgent issue.

This study continues our works on optimization of catalyst performance through regulation of support characteristics [2, 29–34] and it is focused on the elucidation of the role of $Ce_{1-x}M_xO_y$ support composition in physicochemical characteristics of $Ni/Ce_{1-x}M_xO_y$. The regulation of support characteristics and, consequently, the catalyst properties is carried out through a variation of kind (M = Gd, La, Mg) and molar portion (x = 0.1–0.9) of doping cation. Aiming at the identification of composition-structure-property relationships, the prepared samples were characterized by X-ray spectral fluorescence analysis, N_2 adsorption/desorption, X-ray diffraction, transmission electron microscopy, and thermal analysis.

2. Experimental

2.1. Preparation of supports and catalysts

Supports ($Ce_{1-x}Gd_xO_y$, $Ce_{1-x}La_xO_y$, $Ce_{1-x}Mg_xO_y$) were prepared by polymerizable complex method [33, 35]. The x (molar portion of M) was varied from 0.1 to 0.9. For comparative purpose, the one-component oxides (CeO_2, Gd_2O_3, La_2O_3, MgO) were also synthesized in a similar way. The calcination temperature of prepared supports was 500 °C.

The $Ni/Ce_{1-x}M_xO_y$ catalysts (Ni content – 2–15 wt.%) were prepared by incipient wetness impregnation of supports ($Ce_{1-x}Gd_xO_y$, $Ce_{1-x}La_xO_y$, $Ce_{1-x}Mg_xO_y$) with aqueous solutions of nickel nitrate. After that, the samples were dried at 90 °C and calcined in air for 4 h at 500 °C. The number before nickel in the catalyst name corresponds to the Ni content (wt.%).

2.2. Characterization of supports and catalysts

The prepared materials ($Ce_{1-x}M_xO_y$ supports, $Ni/Ce_{1-x}M_xO_y$ catalysts) were characterized by X-ray spectral fluorescence analysis (XRFA), low temperature nitrogen adsorption/desorption, X-ray diffraction (XRD), high resolution transmission electron microscopy (HRTEM) and thermal analysis (TA) in 5%H_2/He in accordance with the procedures described previously [29, 33, 36].

3. Results and discussions

3.1. Characterization of supports

The $Ce_{1-x}Gd_xO_y$, $Ce_{1-x}La_xO_y$ and $Ce_{1-x}Mg_xO_y$ supports were synthesized by the polymerizable complex method. The molar portion of dopant (x) was varied from 0 to 1 and was equal to 0, 0.1, 0.2, 0.5, 0.8, 0.9 and 1.0. The detailed description of properties of the $Ce_{1-x}M_xO_y$ samples with x = 0.1–0.5 can be found in our previous papers [33, 35]. In this work, we increased content of doping cation up to x = 0.8–1.0 and analyzed information for all $Ce_{1-x}M_xO_y$ samples with x = 0–1. The chemical composition of calcined materials determined by X-ray fluorescence spectroscopy was in good agreement with specified value. The specific surface area (S_{BET}) of $Ce_{1-x}M_xO_y$ was changed as a function of the chemical composition of materials in the wide range of values. With an increase of x from 0.1 to 0.9 it decreases from 95 to 20 m^2/g for M = Gd, from 95 to 25 m^2/g for M = La and from 70 to 45 m^2/g for M = Mg. So the S_{BET} has a maximum value at x = 0.1–0.2 and grows in the next series of dopants: La > Gd > Mg. Among one-component samples, the CeO_2 has a relatively high value of S_{BET} – 75 m^2/g, while the specific surface area of the rest was under 25 m^2/g. In particular, it is equal to 15, 25 and 20 m^2/g for Gd_2O_3, La_2O_3 and MgO samples, respectively. The obtained results indicate that the $Ce_{1-x}M_xO_y$ mixed oxides inherit the high S_{BET} of ceria in comparison with M-oxides (M = Gd, La, Mg) and gain the stability against sintering. It is noted that the specific surface area of $Ce_{1-x}M_xO_y$ materials synthesized by the polymerizable complex method is higher than those of samples prepared by sol-gel [37] or citrate complexation [38] methods.

In the applied preparation method metal cations are mixed at the molecular level and are fixed in the polymer matrix the removal of which occurs

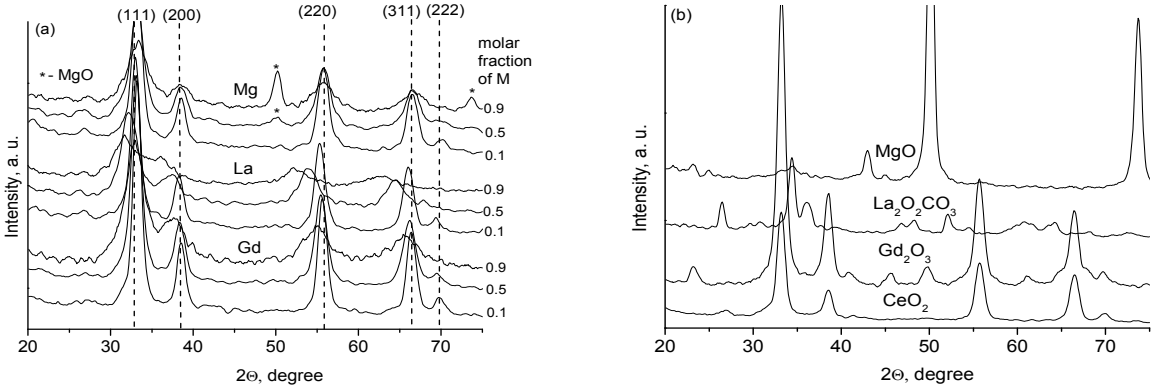

Fig. 1. XRD patterns of $Ce_{1-x}Gd_xO_y$, $Ce_{1-x}La_xO_y$ and $Ce_{1-x}Mg_xO_y$ supports: (a) – x = 0.1; 0.5; 0.9; (b) – x = 0; 1. The broken vertical lines indicate the characteristic peaks of cubic ceria (JCPDS 43-1002).

at low values (300–500 °C) of the calcination temperature [39]. This should ensure the formation of homogeneous solid solutions with developed specific surface area [40]. Indeed, according to XRD data (Fig. 1a), the prepared $Ce_{1-x}M_xO_y$ oxides (x = 0.1–0.9) are single-phase systems with the cubic structure of the fluorite type. The only exception is the Mg-containing system for which at x = 0.5–0.9 the presence of highly dispersed magnesium oxide is observed in addition to the formation of cerium-based oxide (Fig. 1a). The uniform distribution of Gd and La doping cations in $Ce_{1-x}M_xO_y$ (x = 0.1–0.5) matrix was confirmed by EDX maps obtained by the high-angle annular dark-field scanning transmission electron microscopy [35]. The absence of additional La- or Gd-containing phases at x = 0.8–0.9 according to XRD does not exclude their presence in highly dispersed or amorphous state in the composition of the samples.

The partial substitution of Ce^{4+} with Mn^+ is confirmed by shifting of diffraction peaks toward lower (in case of Gd^{3+}, La^{3+}) or higher (in case of Mg^{2+}) angles due to the difference in cation radius of Ce^{4+} (0.97 Å) and those of doping cations M (1.05 Å – Gd^{3+}, 1.16 Å – La^{3+}, 0.72 Å – Mg^{2+}) (Fig. 1a). According to published data [41–46], the cubic fluorite structure of CeO_2 is the sole constituent of the XRD patterns of $Ce_{1-x}M_xO_y$ oxides up to x = 0.4–0.6 for Gd, x = 0.6 for La and x = 0.5–0.9 for Mg-containing solutions. In our case the existence of $Ce_{1-x}Gd_xO_y$ and $Ce_{1-x}La_xO_y$ solid solutions in the wider range of x is connected with the mode (polymerizable complex method vs. co-precipitation) and conditions (low calcination temperature 500 °C vs. 800–1300 °C) of $Ce_{1-x}M_xO_y$ preparation. The phase composition of $Ce_{1-x}M_xO_y$ oxides (x = 0 or 1), which are the one-component systems, after calcination at 500 °C are cerium oxide CeO_2 (x = 0), $La_2O_2CO_3$ lanthanum oxycarbonate (x = 1, M = La), Gd_2O_3 gadolinium oxide (x = 1, M = Gd) and MgO magnesium oxide (x = 1, M = Mg), respectively (Fig. 1b).

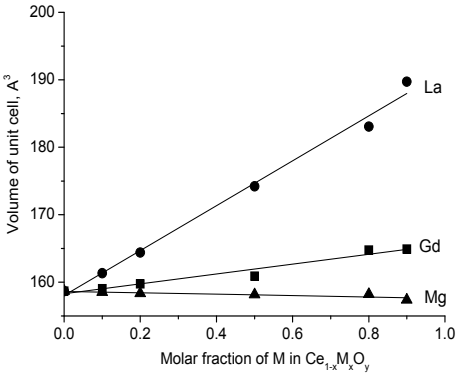

Fig. 2. Average volume of unit cell of $Ce_xM_{1-x}O_y$ supports versus molar fraction (x) of dopant M = Gd, La, Mg.

The volume of the unit cell for $Ce_{1-x}M_xO_y$ is changed in accordance with the radius and content of doping cation. It linearly increases (M = Gd, La) or decreases (M = Mg) with increasing of the molar fraction of the doping cation (Fig. 2).

The average crystallite size (coherent scattering region, CSR) was estimated by applying the Scherrer equation to the characteristic (111) peak of CeO_2 from the XRD. These results indicate that it is sensitive to the molar fraction of doping cations. The size of $Ce_xM_{1-x}O_y$-crystallites dropped to the ~3 nm when the content of doping cation increases (Fig. 3), thus supporting the literature data [44]. According to the HRTEM data [35], the crystallites form polycrystalline agglomerates mainly in the form of plates. The values of CSR are equal to 12 nm, 15 nm and 20 nm for Gd_2O_3, La_2O_3 and MgO samples, respectively.

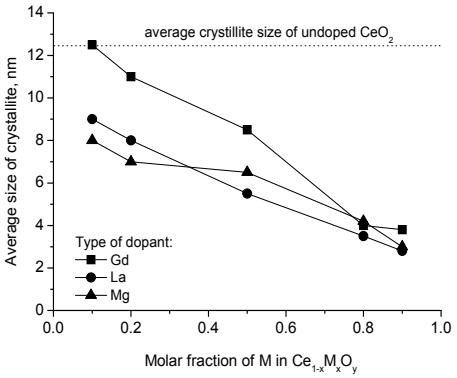

Fig. 3. The crystallite size of $Ce_xM_{1-x}O_y$ supports versus molar fraction (x) of dopant M = Gd, La, Mg.

3.2. Characterization of catalysts

The prepared $Ce_xM_{1-x}O_y$ oxides were used as supports for Ni-containing particles as the active component of reforming catalysts. Compared with S_{BET} of $Ce_xM_{1-x}O_y$ supports, the corresponding S_{BET} value for $Ni/Ce_xM_{1-x}O_y$ catalysts decreases that can be attributed to the blockage of the pores in the support by NiO or some phase transformations. This effect is intensified by increasing of the Ni content in the catalyst composition. Thus, with an increase of Ni content from 2 to 15 wt.% the reduction of the specific surface area increases from 15 to 30% (Fig. 4a). Nevertheless, the tendency in the surface area dependence on the type and content of the dopant was maintained. In particular, higher values of specific surface area are found for Ni catalysts based on $Ce_xM_{1-x}O_y$ supports with a low molar fraction of dopants or containing La as dopant (Fig. 4b, 4c).

At low Ni content (2 and 5 wt.%) XRD patterns of $Ni/Ce_xGd_{1-x}O_y$, $Ni/Ce_xLa_{1-x}O_y$ and $Ni/Ce_xMg_{1-x}O_y$ catalysts with x of 0.1–0.9 showed only the diffraction peaks corresponding to the fluorite type cubic phase of support. There is no evidence of NiO phase in the XRD patterns indicating that in this case NiO species are highly dispersed. At higher Ni loading (10 and 15 wt.%) for $Ni/Ce_xM_{1-x}O_y$ samples the existing phases were cerium-based oxide and Ni-containing phase (Fig. 5a). It is noted that the introduction of nickel does not practically affect the lattice parameter as well as the crystallite size of the CeO_2–based phase of support. With respect to the Ni catalyst supported on the one-component systems (x = 0 or 1) the formation of NiO phase is only found in case of CeO_2 support (Fig. 5b). In the Ni/La_2O_3 samples in addition to $La_2O_2CO_3$ the $LaNiO_3$ phase was formed while in the Ni/Gd_2O_3 and Ni/MgO samples the observed phases were phases of supports – Gd_2O_3 (a mixture of monoclinic and cubic types) and MgO, respectively.

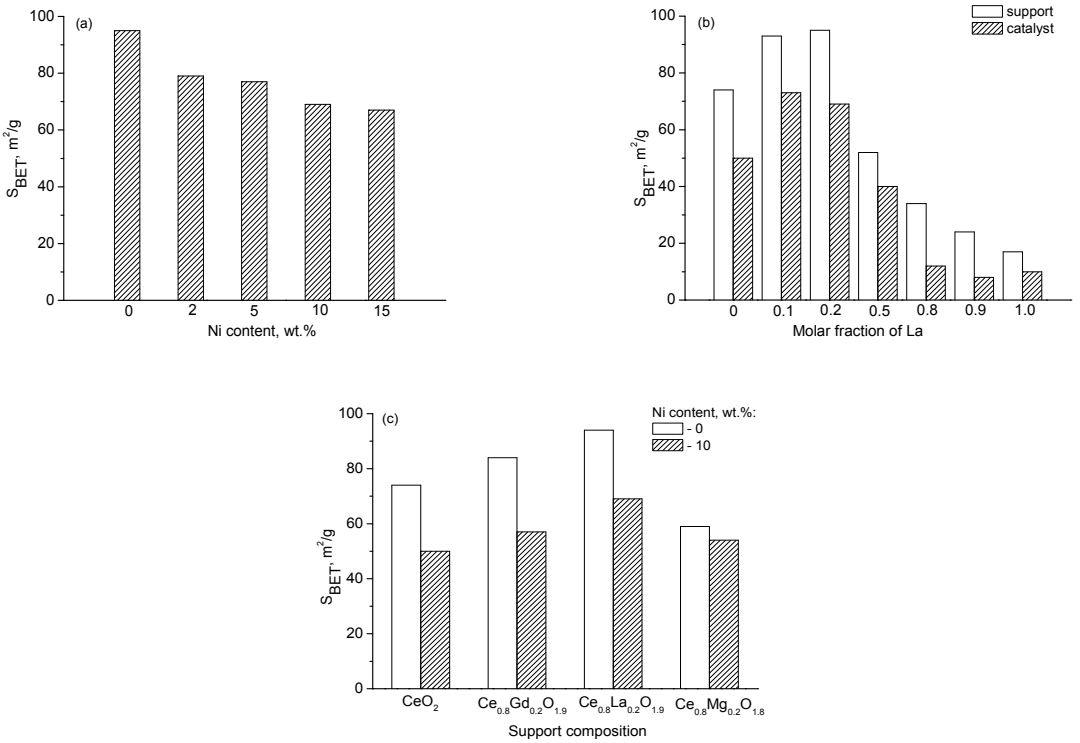

Fig. 4. Effect of Ni content (a) and support composition (b, c) on the specific surface area of $Ni/Ce_xM_{1-x}O_y$ catalysts. For (a) support composition is $Ce_{0.8}La_{0.2}O_{1.9}$.

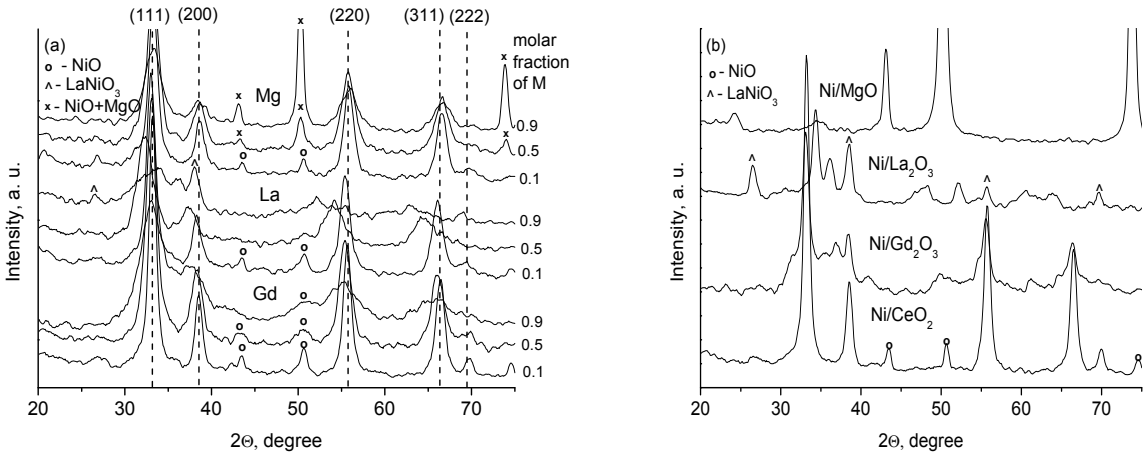

Fig. 5. XRD patterns of $Ni/Ce_xGd_{1-x}O_y$, $Ni/Ce_xLa_{1-x}O_y$ and $Ni/Ce_xMg_{1-x}O_y$ catalysts. Ni content is 10 wt.%: (a) x = 0.1; 0.5; 0.9; (b) x = 0; 1. The broken vertical lines indicate the characteristic peaks of cubic ceria (JCPDS 43-1002).

As follows from the XRD results the chemical composition of $Ce_xM_{1-x}O_y$ has an effect on the kind of supported nickel-containing species which are formed in the support matrix after impregnation and following calcination at 500 °C (Fig. 5a). The Ni-containing species is stabilized in the form of NiO phase (in case of $Ni/Ce_xGd_{1-x}O_y$ with x of 0.1–0.9; in case of $Ni/Ce_xLa_{1-x}O_y$ with x of 0.1–0.8; in case of $Ni/Ce_xMg_{1-x}O_y$ with x of 0.1–0.2) or mixed oxide phase (in case of $Ni/Ce_xLa_{1-x}O_y$ samples with x of 0.9; in case of $Ni/Ce_xMg_{1-x}O_y$ samples with x of 0.5–0.9). Particularly, the XRD spectra of $Ni/Ce_{0.1}La_{0.9}O_{1.55}$ showed the peaks relevant to support and $LaNiO_3$, while the formation of NiO-MgO solid solution is indicated by the value of the lattice parameter of NiO. It was in the range 4.201–4.218 Å which is notably higher than those for "pure" NiO (4.177 Å). The presence of magnesium in the composition of the solid solution based on cerium dioxide (Fig. 1a) contributed to its interaction with nickel and the formation of NiO-MgO solid solution.

It should be noted that irrespective of dopant type the intensity of the XRD line of the NiO phase decreases with an increase of the dopant content (Fig. 5a) that is evidence of decrease of NiO average particle size. This effect is enhanced with a decrease of Ni content and in the following series of samples $Ni/Ce_xMg_{1-x}O_y$ < $Ni/Ce_xGd_{1-x}O_y$ < $Ni/Ce_xLa_{1-x}O_y$ (Fig. 6). So for x = 0.5 the NiO particle size is equal to ~ 7 nm, atomically dispersed state and 15 nm for $10Ni/Ce_{0.5}Gd_{0.5}O_{1.75}$, $10Ni/Ce_{0.5}La_{0.5}O_{1.75}$ and $10Ni/Ce_{0.5}Mg_{0.5}O_{1.7}$ catalysts, respectively. A somewhat different dependence is observed for Mg-containing materials (Fig. 6) that is connected with the stabilization of Ni in different forms: NiO oxide at x = 0–0.2 and NiO-MgO solid solution at x = 0.5–0.9 (Fig. 5a). First, at low values of x in $Ce_xMg_{1-x}O_y$ support the decreasing of NiO particle size occurs, however, with the formation of solid solution at a higher value of x, the size of the Ni-containing phase increases. From the comparison of Fig. 6 and Fig. 4b data it follows that there are no correlation between the particle size of Ni-containing phase and S_{BET} of supports. It can be seen that NiO particle size decreases with the deterioration of the textural characteristics of $Ce_xM_{1-x}O_y$ supports. Thus, the NiO dispersion in the prepared materials is firstly determined by the type and content of dopant.

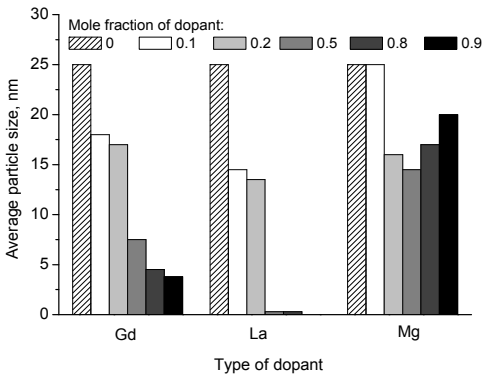

Fig. 6. Effect of support composition on the average particle size of Ni-containing phase in $10Ni/Ce_xM_{1-x}O_y$ catalysts. Ni-containing phase is NiO for $Ni/Ce_xGd_{1-x}O_y$ (x = 0–0.9); $Ni/Ce_xLa_{1-x}O_y$ (x = 0–0.8); $Ni/Ce_xMg_{1-x}O_y$ (x = 0–0.2). Ni-containing phase is NiO-MgO solid solution for M = Mg (x = 0.5–0.9).

It is shown [47] that Rh metal dispersion increases from 47 to 83% when the crystallite size of CeO_2-support was varied from 29.3 to 6.5 nm. Analogously, in our case the growth of dopant content in support composition is accompanied by a decrease of average size of $Ce_xM_{1-x}O_y$-crystallites (Fig. 3) that leads to enhancement of NiO dispersion (Fig. 6). More effective reduction of average particle size of the Ni-containing phase occurs at using of La as a dopant. When the crystallite size of the $Ce_xM_{1-x}O_y$ support is equal to ~4 nm the size of the Ni-containing species is 4.5 nm, atomically dispersed and 17 nm for Gd, La and Mg-containing catalysts, respectively (Fig. 3, Fig. 6). The electron microscopy data confirm the results of the X-ray phase analysis. From TEM images of $10Ni/Ce_{0.2}M_{0.8}O_y$ catalysts (Fig. 7) it follows that the crystallite size of $Ce_{0.2}M_{0.8}O_y$ support is equal to 3–5 nm. The average lattice inter-planar spacing was determined: d = 0.3059 nm in case of $10Ni/Ce_{0.2}Gd_{0.8}O_{1.6}$ sample, d = 0.3229 nm in case of $10Ni/Ce_{0.2}La_{0.8}O_{1.6}$ and d = 0.3058 nm in case of $10Ni/Ce_{0.2}Mg_{0.8}O_{1.2}$. The obtained values of d relate to the crystal face of the doped ceria [48]. The Ni-containing particles with the size of 5–10 nm and 10–20 nm were observed on the surface of $10Ni/Ce_{0.2}Gd_{0.8}O_{1.6}$ (Fig. 7a) and $10Ni/Ce_{0.2}Mg_{0.8}O_{1.2}$, respectively, whereas the $10Ni/Ce_{0.2}La_{0.8}O_{1.6}$ catalyst contains NiO particles with the size of 2 nm (Fig. 7b) and Ni clusters of 0.5 nm in size (Fig. 7c). STEM/EDX elemental mapping confirms the existence of the highly-dispersed species on the $Ce_{0.5}La_{0.5}O_{175}$ support [2]. It is well known that doping of ceria by Gd^{3+}, La^{3+}, Eu^{3+}, Y^{3+}, Pr^{n+}, Sn^{n+} cations or reduction of average size of CeO_2-crystillites provides the growth of concentration of the oxygen vacancies in the mixed oxide [25, 37, 49]. The interaction of active component with such defective sites of support leads to the realization of special interaction between supported species and ceria [48, 50]. So, on the basis of obtained data it can be proposed that the surface defects of $Ce_xM_{1-x}O_y$ serve as centers for stabilization of the Ni-containing active species that preserves them from sintering under thermal treatment and reaction conditions.

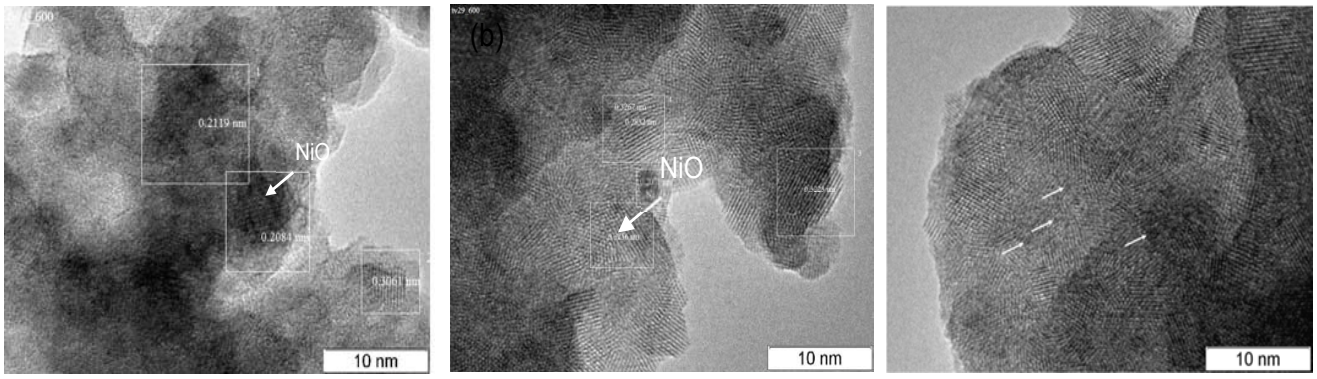

(a) (b) (c)

Fig. 7. TEM images of $10Ni/Ce_{0.2}Gd_{0.8}O_y$ (a) and $10Ni/Ce_{0.2}La_{0.8}O_y$ (b, c) catalysts.

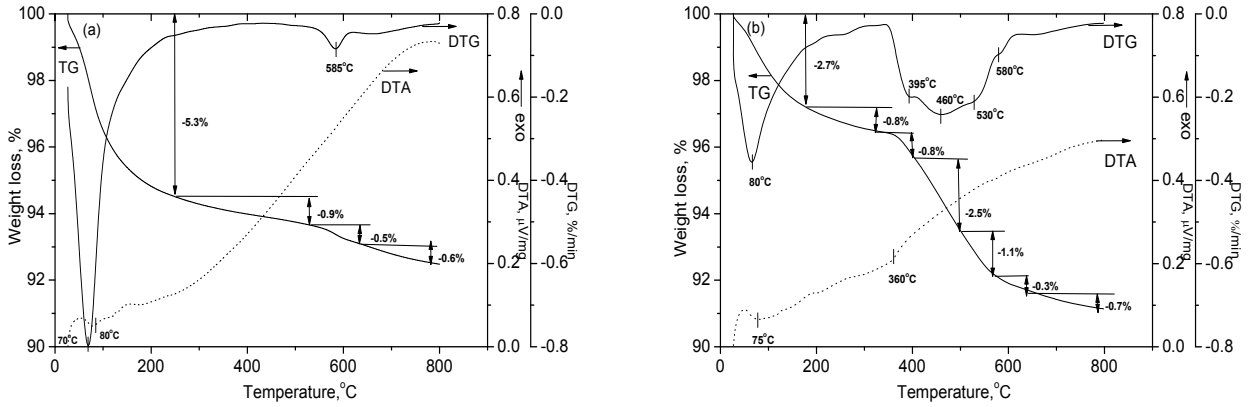

Fig. 8. TG, DTG and DTA curves of $Ce_{0.8}La_{0.2}O_{1.9}$ support (a) and $15Ni/Ce_{0.8}La_{0.2}O_{1.9}$ catalyst (b).

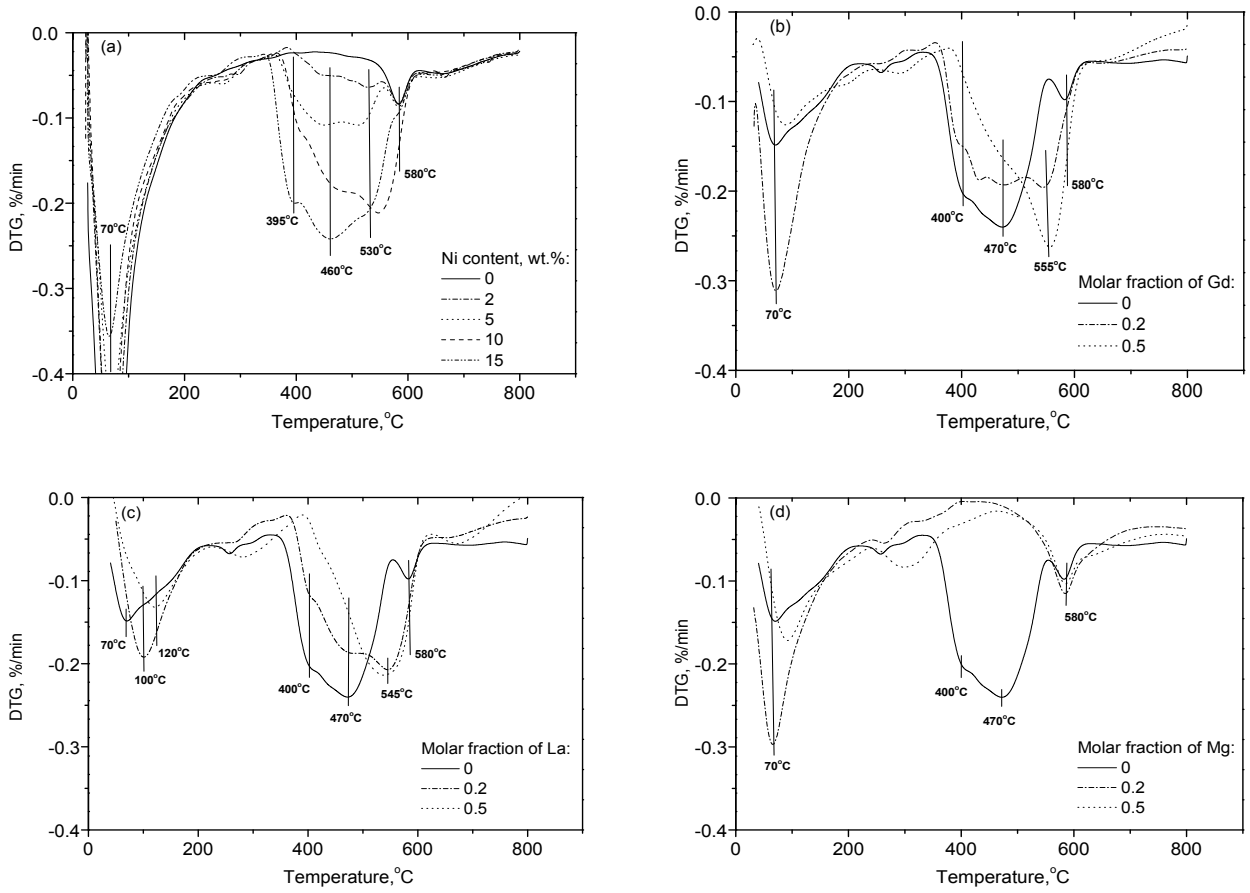

Fig. 9. DTG curves of $Ni/Ce_{0.8}La_{0.2}O_{1.9}$ (a), $10Ni/Ce_{1-x}Gd_xO_y$ (b), $10Ni/Ce_{1-x}La_xO_y$ (c) and $10Ni/Ce_{1-x}Mg_xO_y$ (d) catalysts.

The thermal analysis in $5\%H_2/He$ was carried out to reveal the relationship between the ability to reduction of Ni^{n+} cations and chemical composition of the $Ni/Ce_xM_{1-x}O_y$. As a typical example, Fig. 8 (a, b) shows TG (thermogravimetric), DTG (differential thermogravimetric) and DTA (differential thermal analysis) curves of $Ce_{0.8}La_{0.2}O_{1.9}$ and $15Ni/Ce_{0.8}La_{0.2}O_{1.9}$ samples.

For $Ce_{0.8}La_{0.2}O_{1.9}$ support in the low-temperature region ($T < 200$ °C) an endothermic effect is observed, accompanied by sample weight loss due to the elimination of the adsorbed water. In the high-temperature region, distinct thermic effects do not exist, but the weight loss of the sample occurs at 585 °C ($-\Delta m/m = 0.5$ wt. %). According to H_2-TPR [51], reduction of doped CeO_2 exhibits two regions of hydrogen consumption which may be assigned to the reduction of surface species (300–600 °C) and bulk particles (600–900 °C). It can be assumed that the observed weight loss in the region $T > 200$ °C is related to the reduction of the Ce^{4+} cations, localized on the surface of the particles. TA curves of $15Ni/Ce_{0.8}La_{0.2}O_{1.9}$ catalyst differs from those of $Ce_{0.8}La_{0.2}O_{1.9}$ support, mainly at the temperature range of 350–550 °C where significant weight loss of the sample is observed ($-\Delta m/m$ = 4.4 wt. %) (Fig. 8b). This effect may be connected with Ni^{n+} reduction [52].

The lower Ni content (from 15 to 2 wt. %) leads to the expected decrease in weight changes ($-\Delta m/m$ from 4.4 to 0.8 wt. %) due to the reduction of Ni^{2+} cations (Fig. 9a). Irrespectively of Ni content, there is a peak at 580 °C that is attributed to the reduction of support. Figure 9a shows that with an increase of Ni content a shift towards lower temperatures of the peak connected with NiO reduction occurs. The temperature of the beginning of Ni^{2+} reduction is equal to 400 and 350 °C for 2 wt.% and 15 wt.% samples, respectively. This finding allows us to conclude that reducibility of nickel cations increases with an increase of Ni content in the catalyst. According to [53], it may be connected with the increase of NiO particle size and the decrease of metal-support interaction.

The ability to reduction of nickel cations is changing with variation of $Ce_xM_{1-x}O_y$ support composition (Fig. 9b, 9c, 9d). In particular, among studied materials the least ability to reduction is

observed for Ni/$Ce_{1-x}Mg_xO_y$ (Fig. 9d) that can be related with the existence of NiO-MgO solid solution in these samples (Fig. 5) [54]. Regardless of the type of the dopant, an increase in its content leads to an increase in the proportion of hard-to-reduce forms of nickel cations (Fig. 9b, 9c).

It can be concluded that growth of x value from 0.1 to 0.9 for $Ce_{1-x}Gd_xO_y$, $Ce_{1-x}La_xO_y$ or and $Ce_{1-x}Mg_xO_y$ supports leads to improving the interaction between the supported species of active component and carrier due to the reduction of the crystallite size of the $Ce_xM_{1-x}O_y$ and increase of the concentration of surface defects. Such increase in the degree of metal-support interaction is manifested in increase of the dispersion of the Ni species, but also in the deterioration of its reducibility. The identified variation of the textural, structural and redox characteristics of the Ni/$Ce_xM_{1-x}O_y$ catalysts should influence their performance in the catalytic process.

4. Conclusions

Nickel catalysts on $Ce_{1-x}M_xO_y$ supports were prepared by incipient wetness impregnation method, and their physicochemical properties were studied against Ni content (0–15 wt.%) and composition of support ($Ce_xGd_{1-x}O_y$, $Ce_xLa_{1-x}O_y$ and $Ce_xMg_{1-x}O_y$, x = 0–1). The increase of the dopant content in $Ce_xM_{1-x}O_y$ solid solution induces the decrease of its crystallite size and strengthens the Ni-support interaction. It causes improvement of Ni dispersion but decreases Ni^{n+} cation reducibility. It is expected that Ni/$Ce_{1-x}M_xO_y$ catalyst performance in reforming of fuels will be optimized by selection of appropriate support composition.

Acknowledgments

This work was supported by the RFBR project No. 18-53-45012 India.

References

[1]. S. De, J. Zhang, R. Luque, N. Yan, *Energy Environ. Sci.* 9 (2016) 3314–3347. DOI: 10.1039/c6ee02002j.

[2]. Z.R. Ismagilov, E. V Matus, I.Z. Ismagilov, O.B. Sukhova, S.A. Yashnik, V.A. Ushakov, M.A. Kerzhentsev, *Catal. Today* (2018) 0–1. DOI: 10.1016/j.cattod.2018.06.035.

[3]. R. Amin, B. Liu, Z.B. Huang, Y.C. Zhao, *Int. J. Hydrogen Energy* 41 (2016) 807–819. DOI: 10.1016/j.ijhydene.2015.10.063.

[4]. H. Li, H. Xu, J. Wang, *J. Nat. Gas Chem.* 20 (2011) 1–8. DOI:10.1016/S1003-9953(10)60156-9.

[5]. Z. Alipour, M. Rezaei, F. Meshkani, *Fuel* 129 (2014) 197–203. DOI: 10.1016/j.fuel.2014.03.045.

[6]. G. Nahar, V. Dupont, *Sustain. Energy Rev.* 32 (2014) 777–796. DOI: 10.1016/j.rser.2013.12.040.

[7]. Z. Wei, J. Sun, Y. Li, A.K. Datye, Y. Wang, *Chem. Soc. Rev.* 41 (2012) 7994. DOI: 10.1039/c2cs35201j.

[8]. J. Requies, V.L. Barrio, J.F. Cambra, M.B. Güemez, P.L. Arias, V. La Parola, M.A. Peña, J.L.G. Fierro, *Fuel* 87 (2008) 3223–3231. DOI: 10.1016/j.fuel.2008.05.004.

[9]. C. Pirez, W. Fang, M. Capron, S. Paul, H. Jobic, F. Dumeignil, L. Jalowiecki-Duhamel, *Appl. Catal. A Gen.* 518 (2016) 78–86. DOI: 10.1016/j.apcata.2015.10.035.

[10]. S.C. Dantas, K.A. Resende, C.N. Ávila-Neto, F.B. Noronha, J.M.C. Bueno, C.E. Hori, *Int. J. Hydrogen Energy* 41 (2016) 3399–3413. DOI: 10.1016/j.ijhydene.2015.12.164.

[11]. A.C. Furtado, C.G. Alonso, M.P. Cantão, N.R.C. Fernandes-Machado, *Int. J. Hydrogen Energy.* 36 (2011) 9653–9662. DOI: 10.1016/j.ijhydene.2011.05.063.

[12]. H. V. Fajardo, E. Longo, D.Z. Mezalira, G.B. Nuernberg, G.I. Almerindo, A. Collasiol, L.F.D. Probst, I.T.S. Garcia, N.L. V Carreño, *Environ. Chem. Lett.* 8 (2010) 79–85. DOI: 10.1007/s10311-008-0195-5.

[13]. T.S. Moraes, R.C. Rabelo Neto, M.C. Ribeiro, L.V. Mattos, M. Kourtelesis, S. Ladas, X. Verykios, F.B. Noronha, *Appl. Catal. B Environ.* 181 (2016) 754–768. DOI: 10.1016/j.apcatb.2015.08.044.

[14]. M.C. Sánchez-Sánchez, R.M. Navarro, J.L.G. Fierro, *Int. J. Hydrogen Energy* 32 (2007) 1462–1471. DOI: 10.1016/j.ijhydene.2006.10.025.

[15]. M. Muñoz, S. Moreno, R. Molina, *Int. J. Hydrogen Energy* 39 (2014) 10074–10089. DOI: 10.1016/j.ijhydene.2014.04.131.

[16]. O. Akdim, W. Cai, V. Fierro, H. Provendier, A. van Veen, W. Shen, C. Mirodatos, *Top. Catal.* 51 (2008) 22–38. DOI: 10.1007/s11244-008-9122-z.

[17]. S.Q. Chen, Y. Liu, *Int. J. Hydrogen Energy* 34 (2009) 4735–4746. DOI: 10.1016/j.ijhydene.2009.03.048.

[18]. F. Liu, L. Zhao, H. Wang, X. Bai, Y. Liu, *Int. J. Hydrogen Energy* 39 (2014) 10454–10466. DOI: 10.1016/j.ijhydene.2014.05.036.

[19]. R. Trane-Restrup, S. Dahl, A.D. Jensen, *Int. J. Hydrogen Energy* 38 (2013) 15105–15118. DOI: 10.1016/j.ijhydene.2013.09.027.

[20]. M. Ni, D.Y.C. Leung, M.K.H. Leung, *Int. J. Hydrogen Energy* 32 (2007) 3238–3247. DOI: 10.1016/j.ijhydene.2007.04.038.

[21]. P. Osorio-Vargas, N.A. Flores-González, R.M. Navarro, J.L.G. Fierro, C.H. Campos, P. Reyes,

Catal. Today 259 (2016) 27–38. DOI: 10.1016/j.cattod.2015.04.037.
[22]. J.A. Farmer, C.T. Campbell, *Science* 329 (2010) 933–936. DOI: 10.1126/science.1191778.
[23]. R. Pérez-Hernández, A. Gutiérrez-Martínez, J. Palacios, M. Vega-Hernández, V. Rodríguez-Lugo, *Int. J. Hydrogen Energy* 36 (2011) 6601–6608. DOI: 10.1016/j.ijhydene.2011.02.064.
[24]. X. Han, Y. Yu, H. He, J. Zhao, Y. Wang, *J. Power Sources* 238 (2013) 57–64. DOI: 10.1016/j.jpowsour.2013.03.032.
[25]. W.Y. Hernández, O.H. Laguna, M.A. Centeno, J.A. Odriozola, *J. Solid State Chem.* 184 (2011) 3014–3020. DOI: 10.1016/j.jssc.2011.09.018.
[26]. J. Paier, C. Penschke, J. Sauer, *Chem. Rev.* 113 (2013) 3949–3985. DOI: 10.1021/cr3004949.
[27]. F.L.S. Carvalho, Y.J.O. Asencios, A.M.B. Rego, E.M. Assaf, *Appl. Catal. A Gen.* 483 (2014) 52–62. DOI: 10.1016/j.apcata.2014.06.027.
[28]. X. Han, Y. Yu, H. He, W. Shan, I*nt. J. Hydrogen Energy* 38 (2013) 10293–10304. DOI: 10.1016/j.ijhydene.2013.05.137.
[29]. I.Z. Ismagilov, E. V. Matus, V.V. Kuznetsov, N. Mota, R.M. Navarro, M.A. Kerzhentsev, Z.R. Ismagilov, J.L.G. Fierro, *Catal. Today* 210 (2013) 10–18. DOI: 10.1016/j.cattod.2012.12.007.
[30]. I.Z. Ismagilov, E.V. Matus, V.V. Kuznetsov, M.A. Kerzhentsev, S.A. Yashnik, I.P. Prosvirin, N. Mota, R.M. Navarro, J.L.G. Fierro, Z.R. Ismagilov, *Int. J. Hydrogen Energy* 39 (2014) 20969–20983. DOI: 10.1016/j.ijhydene.2014.10.044.
[31]. I.Z. Ismagilov, E.V. Matus, D.V. Nefedova, V.V. Kuznetsov, S.A. Yashnik, M.A. Kerzhentsev, Z.R. Ismagilov, *Kinet. Catal.* 56 (2015) 394–402. DOI: 10.1134/S0023158415030064.
[32]. N. Mota, I.Z. Ismagilov, E.V. Matus, V.V. Kuznetsov, M.A. Kerzhentsev, Z.R. Ismagilov, R.M. Navarro, J.L.G. Fierro, *Int. J. Hydrogen Energy* 41 (2016) 19373–19381. DOI: 10.1016/j.ijhydene.2016.05.029.
[33]. E.V. Matus, D.V. Nefedova, V.V. Kuznetsov, V.A. Ushakov, O.A. Stonkus, I.Z. Ismagilov, M.A. Kerzhentsev, Z.R. Ismagilov, *Kinet. Catal.* 58 (2017) 610–621. DOI: 10.1134/S0023158417050160.
[34]. I.Z. Ismagilov, E.V. Matus, V.V. Kuznetsov, S.A. Yashnik, M.A. Kerzhentsev, G. Gerritsen, H.C.L. Abbenhuis, Z.R. Ismagilov, *Eurasian Chemico-Technological Journal* 19 (2017) 3–16. DOI: 10.18321/ectj497
[35]. M.A. Kerzhentsev, E.V. Matus, I.Z. Ismagilov, V.A. Ushakov, O.A. Stonkus, T.V. Larina, G.S. Kozlova, P. Bharali, Z.R. Ismagilov, *J. Struct. Chem.* 58 (2017) 133–141. DOI: 10.1134/S002247661701019X.
[36]. I.Z. Ismagilov, E. V. Matus, V.V. Kuznetsov, N. Mota, R.M. Navarro, S.A. Yashnik, I.P. Prosvirin, M.A. Kerzhentsev, Z.R. Ismagilov, J.L.G. Fierro, *Appl. Catal. A Gen.* 481 (2014) 104–115. DOI: 10.1016/j.apcata.2014.04.042.
[37]. B. Zhang, D. Li, X. Wang, *Catal. Today* 158 (2010) 348–353. DOI:10.1016/j.cattod.2010.04.019.
[38]. R.O. Fuentes, R.T. Baker, *J. Power Sources.* 186 (2009) 268–277. DOI: 10.1016/j.jpowsour.2008.09.119.
[39]. S. Sakka, H. Kozuka, Handbook of sol-gel science and technology, Vol. 1, Sol-gel processing, 2005.
[40]. M. Rezaei, S.M. Alavi, S. Sahebdelfar, Z.F. Yan, J. Porous Mater. 16 (2009) 497–505. DOI: 10.1007/s10934-008-9224-9.
[41]. J. Zhang, C. Ke, H. Wu, J. Yu, J. Wang, Y. Wang, *J. Alloys Compd.* 718 (2017) 85–91. DOI: 10.1016/j.jallcom.2017.05.073.
[42]. C. Peng, Z. Zhang, *Ceram. Int.* 33 (2007) 1133–1136. DOI: 10.1016/j.ceramint.2006.03.004.
[43]. W. Gong, R. Zhang, Z. Chen, *Trans. Nonferrous Met. Soc. China.* 21 (2011) 2671–2676. DOI: 10.1016/S1003-6326(11)61109-6.
[44]. M.F. Wilkes, P. Hayden, A.K. Bhattacharya, *J. Catal.* 219 (2003) 305–309. DOI: 10.1016/S0021-9517(03)00046-0.
[45]. M. Chen, H. Zheng, C. Shi, R. Zhou, X. Zheng, *J. Mol. Catal. A Chem.* 237 (2005) 132–136. DOI: 10.1016/j.molcata.2005.04.038.
[46]. V.K. Nguyen, J.H. Park, C.H. Shin, *React. Kinet. Mech. Catal.* 107 (2012) 157–165. DOI: 10.1007/s11144-012-0451-3.
[47]. J. Kugai, V. Subramani, C. Song, M.H. Engelhard, Y.H. Chin, *J. Catal.* 238 (2006) 430–440. DOI: 10.1016/j.jcat.2006.01.001.
[48]. F. Wang, L. Xu, J. Yang, J. Zhang, L. Zhang, H. Li, Y. Zhao, H.X. Li, K. Wu, G.Q. Xu, W. Chen, *Catal. Today* 281 (2017) 295–303. DOI: 10.1016/j.cattod.2016.03.055.
[49]. G. Xiao, S. Li, H. Li, L. Chen, *Microporous Mesoporous Mater.* 120 (2009) 426–431. DOI: 10.1016/j.micromeso.2008.12.015.
[50]. D. Li, X. Li, J. Gong, *Chem. Rev.* 116 (2016) 11529–11653. DOI: 10.1021/acs.chemrev.6b00099.
[51]. X. Yao, C. Tang, Z. Ji, Y. Dai, Y. Cao, F. Gao, L. Dong, Y. Chen, *Catal. Sci. Technol.* 3 (2013) 688–698. DOI: 10.1039/C2CY20610B.
[52]. J.A. Montoya, E. Romero-Pascual, C. Gimon, P. Del Angel, A. Monzon, *Catal. Today* 63 (2000) 71–85. DOI: 10.1016/S0920-5861(00)00447-8.
[53]. P. Biswas, D. Kunzru, *Int. J. Hydrogen Energy* 32 (2007) 969–980. DOI: 10.1016/j.ijhydene.2006.09.031.
[54]. G.T. Wurzler, R.C. Rabelo-Neto, L.V. Mattos, M.A. Fraga, F.B. Noronha, *Appl. Catal. A Gen.* 518 (2016) 115–128. DOI: 10.1016/j.apcata.2015.11.020.